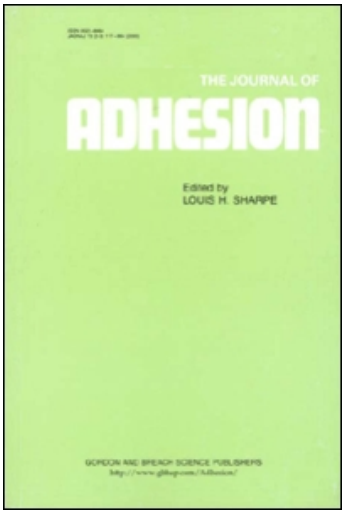

The Journal of Adhesion
Publication details, including instructions for authors and subscription information:
http://www.informaworld.com/smpp/title~content=t713453635

The Effects of Laser Radiation at 248 nm on the Surface Characteristics and Joint Properties of Aluminum Adherends

E. Sancaktar[a]; S. V. Babu[a]; E. Zhang[a]; G. C. D'Couto[a]; H. Lipshitz[b]
[a] Center for Advanced Materials Processing, Clarkson University, Potsdam, NY, USA [b] Derma-Metrics, Bedford, MA, USA

To cite this Article Sancaktar, E. , Babu, S. V. , Zhang, E. , D'Couto, G. C. and Lipshitz, H.(1995) 'The Effects of Laser Radiation at 248 nm on the Surface Characteristics and Joint Properties of Aluminum Adherends', The Journal of Adhesion, 50: 2, 103 — 133
To link to this Article: DOI: 10.1080/00218469508014361
URL: http://dx.doi.org/10.1080/00218469508014361

J. Adhesion, 1995, Vol. 50, pp. 103–133
Reprints available directly from the publisher
Photocopying permitted by license only

The Effects of Laser Radiation at 248 nm on the Surface Characteristics and Joint Properties of Aluminum Adherends*

E. SANCAKTAR**, S. V. BABU, E. ZHANG, G. C. D'COUTO

Center for Advanced Materials Processing, Clarkson University, Potsdam, NY 13699-5729, USA

H. LIPSHITZ

Derma-Metrics, 18 North Road, Bedford, MA 10730, USA

(Received June 25, 1994; in final form December 12, 1994)

Procedures presently used to prepare surfaces of aluminum adherends for bonding with structural adhesives entail the use of corrosive solutions that are environmentally hazardous.

As an alternative, we investigated whether eximer laser radiation can effectively be used to prepare the surfaces of aluminum adherends. The results indicate such a methodology to be very promising. Using a KrF laser, at a radiant intensity of 1.67×10^{13} W/m^2/pulse, successive mm^2 regions of aluminum coupons were irradiated for fixed numbers of pulses/region. This resulted in changes to the topographies and oxidation states of the surfaces. Symmetric lap shear joints from coupons so treated had considerably increased strains at fracture and 24% greater joint strengths as compared with controls. The results further indicate that fracture toughness can be increased above that of presently used procedures. The topographies of the treated and control surfaces were characterized using a new topographic characterizing system. An elastic model is presented that relates failure characteristics to experimentally-determined topographic parameters. The results suggest that different mechanisms for joint enhancement are operative.

KEY WORDS: eximer laser; surface preparation; adhesion; fracture toughness; surface topography; oxidation; fracture mechanisms; interphase; mechanical adhesion; aluminum substrates.

I. INTRODUCTION

Surface preparation is required for attaining joint durability and high joint strengths with aluminum adherends.[1–3] The procedures commonly used, particularly for aerospace applications, are either etching or anodization in acid solutions.[1–3] These remove weak boundary layers, cause changes to the metal's surface energetics (primarily through oxidation) and its microtopographical characteristics. The net effects of these changes are enhanced interfacial bonding, mechanical interlocking between adhesive and metal[1–4] and greater resistance to environmental degradation by moisture or humidity.[1] Details of the various methodologies, as well as their advantages and

* Presented in part at the Sixteenth Annual Meeting of The Adhesion Society, Inc., Williamsburg, Virginia, U. S. A., February 21–26, 1993.

** Corresponding author.

disadvantages, have been reviewed by Clearfield and McNamara,[1] Wegman[2], and Thrall and Shannon.[3]

A common feature of all these procedures, however, is the use of corrosive solutions. These are environmentally hazardous and cumbersome to use when preparing surfaces of large workpieces. We, therefore, sought other methodologies for surface preparation that might likewise improve joint properties.

As known, laser radiation of sufficient energy can affect material surfaces in various ways.[5–11] As such, it has found use in a variety of industrial processes.[5,6] Relatively recently, excimer lasers* that emit relatively high energy pulses of very short duration in the UV became commercially available. The radiation from these lasers couples strongly with metals[5,12] and offers the promise of affecting precise, controllable changes to the morphologies, oxidation states, and other properties of metal surfaces.

More specifically, the irradiation of an aluminum-copper alloy with a KrF excimer laser was shown to change its surface lattice parameters. Other surface effects reported include topographical changes,[11,12] annealing,[13] alloy formation[14] and surface oxidation.[12,15,16] Therefore, we decided to explore the use of eximer laser radiation for preparing the surfaces of aluminum adherends.

In these studies, aluminum coupons were irradiated under different conditions with a KrF eximer laser emitting at 248 nm. The compositional and topographic characteristics of the surfaces were analyzed. Then, the differently irradiated samples were adhered to form symmetric single lap joints using a commercial epoxy adhesive and the mechanical characteristics of the joints determined under shear. It is the subject of this communication to relate the surface characteristics obtained to the changes in joint properties.

A similar effort was recently reported by Dodiuk** *et al.*[17] These investigators, apparently similarly motivated, used an ArF eximer laser, emitting at 193 nm, and different radiation procedures to prepare the surfaces of aluminum adherends. Their experimental procedures and results differed from ours and these differences are discussed in greater detail in the discussion section. We would note, however, at this point, that those aluminum adherends subjected to their radiation procedures exhibited considerably greater joint strengths as compared with controls. As such, their work is supportive of the use of excimer laser radiation as a methodology for surface preparation.

As known, many processes can occur, each at different rates, when a material is subjected to high-energy laser radiation.[5,8] These can include, among other effects, material losses through vaporization or ablation,[18,19] molten flow,[13,20] chemical reactions between laser-induced plasma constituents and the surface[21] and between dissolved species and the metal.[22] Clearly, the entire process is complex and we have

* Excimer lasers are lasers based on molecular emissions from strongly-bound excited state molecules to weakly-bound, unstable ground states. Lasers utilizing the rare gas halides (such as krypton fluoride (KrF), argon fluoride (ArF), etc.) are a subclass of excimer lasers.[5]

** The work of Dodiuk *et al.*[17] was not yet in print when our manuscript was initially submitted. Their manuscript was graciously furnished to us by the Editor of this journal, just prior to its publication, so that we could refer to it during revisions. Our two groups, therefore, approached this problem independently, but from a similar perspective.

not, as yet, worked out the details of relating radiation conditions to surface properties. Our results should, therefore, not be taken as optimum but rather as effects attained under specified conditions. It is our purpose to explain the relationships between the surface morphologies and oxidation states obtained and the greater joint strengths and extensibilities observed.

II. PROCEDURES

A. Materials Used

1. Aluminum

1.5 mm thick 2024 Aluminum coupons were used throughout this investigation.

2. Adhesive

The adhesive was a commercial, high-modulus, high-strength, epoxy adhesive of proprietary composition, that is commonly used in the aerospace industry. The adhesive, made by The Aerospace and Industrial Products Division of Dexter Hysol of California, USA, is sold under the commercial name of Hysol EA 9628 NW Solid Film Adhesive.

The heating protocol affecting cure was that recommended by the manufacturer. This consisted of raising the temperature of the adhesive at a rate of 2.8°C/min until a temperature of 121°C was attained. The temperature was then held constant for 60 minutes.

All joint specimens, including the controls (*i.e.* no laser treatment) were prepared with this adhesive system.

B. Surface Preparative Procedures

1. Laser Radiation Procedure

a. Laser

The laser used was a KrF eximer laser, emitting at 248 nm. The system, an EMG 101 laser, was obtained from Lambda Physik of Germany. It emits a beam having an unfocused cross-sectional area of 2 cm^2. Pulses of 15 ns duration, having an energy of 250 mJ/pulse, are emitted at frequencies that can range from 1 to 100 Hz. For all experiments in this work, the laser was operated at 2 Hz. The average energy per pulse was measured with a Gentec joulemeter.

In the procedures to be described, each region was irradiated for a designated number of pulses. The short pulse duration, coupled with the very rapid cooling rates attained with such laser radiation[22] because only surface heating is involved, assured that surface changes due to each pulse were complete before the metal was subjected to another pulse.

b. Radiation Protocols

Radiation of entire bonded areas was attained by stepwise irradiation of 1 × 1 mm regions. The laser beam was focused through a magnesium fluoride coated quartz lens (Acton Research Corp., Acton, MA, USA) such that 1 mm^2 regions were irradiated at a time. The transmission efficiency of the lens was 94%.

The average radiant intensity incident on each mm^2 was roughly 1.67×10^{13} W/m^2. This is greater than the intensities required for melting, I_m, (1.49×10^{12} W/m^2) or vaporization, I_v, (5.66×10^{12} W/m^2) as calculated by the procedures of Breinon and Keal.[23] Further, the times required for the surface to reach temperatures for melting and vaporization are calculated to be approximately 0.12 and 1.72 ns, respectively, or from 1 to 11.5% of the pulse duration. Note that absorbance decreases rapidly with depth in metals.

Stepwise irradiation was facilitated by a computer-controlled x, y motorized stage (Fig. 1), controlled by a programmable modular automation controller (Model MACX200) Techno, DSG Company (New Hyde Park, New York, USA).

The procedure was as follows. Prior to irradiation the samples were degreased by immersions in acetone and air dried. The samples were affixed to the stage and positioned perpendicular to the laser beam (Fig. 1). Following the irradiation of a mm^2 region for the designated number of pulses (either 5 or 20) the sample was moved to a juxtaposed region and likewise irradiated for the same number of pulses. The process was repeated until a "line" of mm^2 regions was so exposed. There was no overlap of irradiated regions.

A "line" of 25 square regions was irradiated, following which the sample was moved to a position below the last and the process repeated for 8 juxtaposed lines. Thus, 200 such regions were irradiated (*i.e.*, 8 lines of 25 regions each) covering an area of 8 mm × 25 mm.

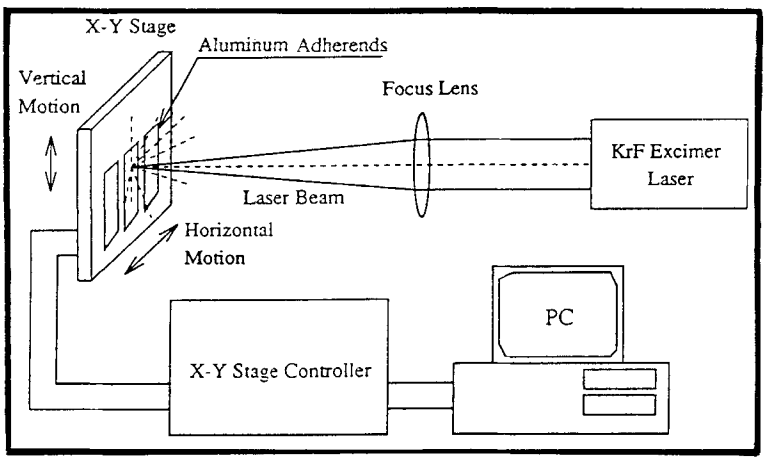

FIGURE 1 Schematic diagram of the apparatus used for the laser irradiation of aluminum coupons.

2. Chromic Acid Anodization

Chromic acid anodization (CAA) was done on untreated surfaces for the purpose of comparing their effects on joint properties (with those subjected to laser treatment). CAA, as known, is a frequently used surface preparative procedure for aluminum adherends.[13]

The procedures used are delineated in Table I.

Specimens treated chemically or by irradiation were stored in a vacuum desiccator for no longer than 2 days.

C. Preparation of Joint Specimens and Mechanical Testing Procedures

Two groups of symmetric single lap joint specimens (see Fig. 2) were prepared as follows.

GROUP I consisted of 2 subgroups of 3 or 4 samples each, having a bonded area of 8 mm × 25 mm. The subgroups were a "control" group (surfaces not exposed to the laser) and a group subjected to 20 pulses/region. The pressure during cure for Group I was 175 kPa. At this pressure, the initial adhesive film thickness of 0.254 mm was reduced to an average thickness of 0.225 mm.

GROUP II comprised 3 subgroups of 3 or 4 samples each having a bonded area of 8 mm × 25 mm. One was the control group, one was exposed to 20 p/reg, and the third was treated with CAA. The pressure for Group II was roughly double (345 kPa) that for Group I. This resulted in an average adhesive thickness of 0.14 mm.

The bonding procedure was as follows. A strip of the Hysol EA 9628 NW solid film adhesive having the same dimensions as the bonded areas was sandwiched between the two surfaces. The joints of Groups I and II were subjected to 175 KPa and 345 kPa

TABLE I
Chemical Treatment for Aluminum Adherends

FPL pretreatment	
1. Solvent degrease	1,1,1-trichloroethane
2. Alkaline deoxidize	Turco 4215S
3. Rinse, 5 min, RT	Water
4. Etch, 65°C	FPL solution 60 g/L $Na_2Cr_2O_7$–$2H_2O$, 173 g/L 96% H_2SO_4, 1.9 g/L 2024 Al, bal water
5. Rinse	Deionized water
6. Oven dry	
CAA treatment (Bell Helicopter)	
1. FPL pretreatment	
2. Anodization	60–100 g/L CrO_3, 33–37°C 3–5 V/min to 40 V, hold 30–35 min.
3. Rinse	1–5 min 20°C, Oven dry (< 65°C)

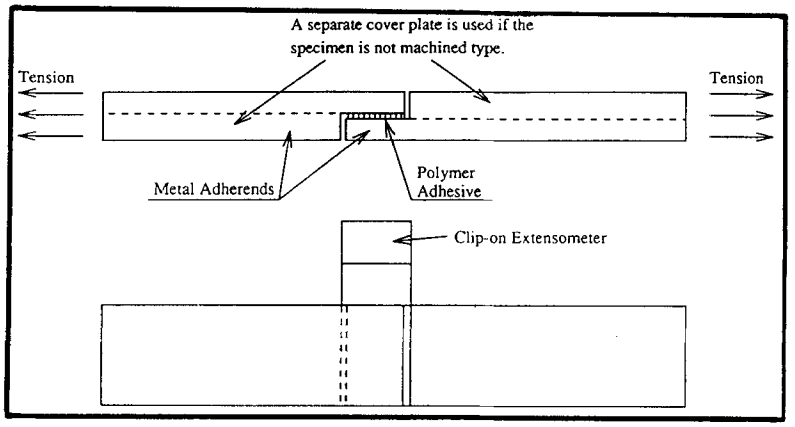

FIGURE 2 Schematic diagram of joint geometry used for testing with clip-on extensometer.

pressure (respectively) while being heated at the rates described earlier to affect cure. All joints subsequent to preparation were equilibrated against air maintained at 22.7°C and 60% relative humidity for around 2 days prior to testing.

Mechanical testing was done with a model 1331 Instron Universal Testing Machine (Instron Instrument Co., Canton, MA, USA) at an extension rate of 5 mm/min. The joints were strained to failure and the loads, extensions at failure, and mode of failure noted. All testing was done under the controlled environmental conditions of 60% RH and 22.7°C.

Stress-strain curves for joints prepared from control, CAA-treated and totally-irradiated surfaces (20 p/reg) were obtained. Best fit curves for these data (averaged over three or four determinations), are shown along with representative data points in Figures 3A and 3B for Groups I and II, respectively. These curves were obtained by a bimodal curve-fitting procedure which utilized a linear fit for the initial portion and the data points shown are obtained from digital output data of the Instron mechanical testing machine. We should note that the data points shown include the extreme values for the stress-strain experiments.

D. Characterization Procedures

1. Topographic Characterization

Topographic characterization of the control and irradiated surfaces was done using scanning electron microscopy (SEM) and a mechano-optical system (described below) for quantitative topographic characterization.[24,25]

a. Scanning Electron Microscopy

Scanning electron micrographs were obtained using a JEOL JSM-6300 scanning electron microscope, (JEOL, Japan). The sample surfaces were sputter-coated with

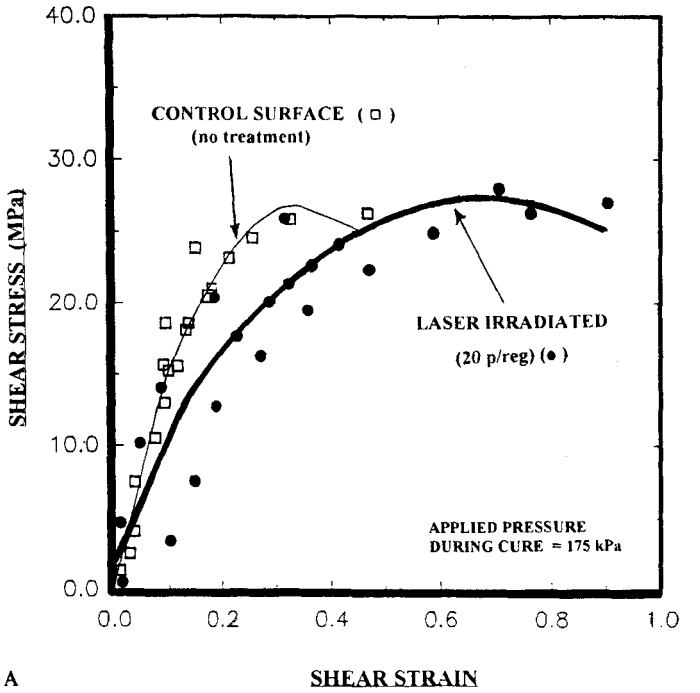

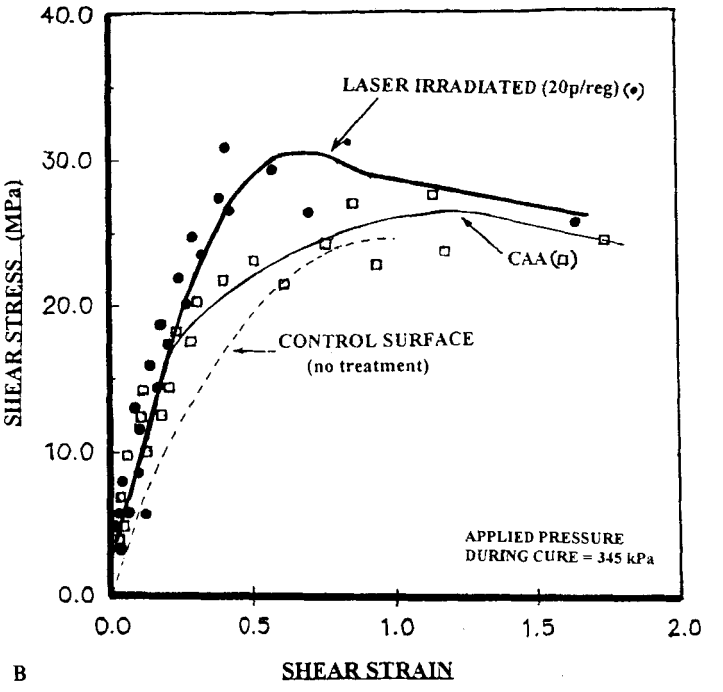

FIGURE 3A and B. Stress-strain diagrams for untreated and laser-irradiated joints (20 p/reg) using the same adhesive and cured under 175 kPa pressure (A), 345 kPa pressure (B). The distribution of data points for the control sample in (B) is similar to that in (A).

gold and viewed under an excitation voltage of 15 KV. The resolution of this SEM is 4 nm.

b. Quantitative Topographic Characterization

(1) Data Description and Acquisition Procedures

Quantitative topographic characterization was done using the mechano-optical system alluded to above. In this system, the primary data obtained are the heights, z, as a function of their x, y coordinates in a reference plane (*i.e.*, $z = z(x, y)$). The data are obtained over a rectangular area where the intervals between coordinate points are an experimental variable. z-values are initially obtained with respect to an instrument reference plane but are then transformed, by appropriate processing, to functions of x, y coordinates in the midplane bisecting the heights of the area that is reoriented parallel to the instrument reference plane.[24] All the height data are reported with respect to the same common reference plane, *i.e.*, $z = 0$, and all heights are either above (*i.e.*, $(+)$) or below (*i.e.*, $(-)$) the mean regression plane. Positions on the plane have the height 0. All statistical and geometric parameters derive from operations on the matrix $z(x, y)$. Thus, all characteristic parameters and distribution functions are computed from area[25] as opposed to profile data.

When using this method, the distances between points can range from 0.3μ to many microns and heights can be resolved to within 0.3μ. Details of the procedures are described in References 24 and 25.

(2) Facsimile Images

Three-dimensional plots of coordinate data so obtained result in facsimile images that are in excellent agreement with optical and scanning electron micrographs of the same region. However, by enlarging the z-axis scale, relative to the x, y axes, one can visualize surface features over much wider fields than is possible with optical or electron micrographs.

(3) Surface Inclination Histograms

The distributions of surface inclinations for irradiated and control samples are characterized as follows. The surfaces are modeled as triangular polyhedra (*i.e.*, surfaces consisting of triangles, imagined to be "glued together" (Fig. 4)).

Two legs of each successive triangle constitute vectors whose cross product, normal to the triangular plane, make an angle, θ, with the midplane (Fig. 4). In this model, the angles can range from 0° to 90° with only integral values considered (no account is taken of the azimuthal directions of the cross product vector—only the acute angles made with the midplane). We term the angles between the cross product vectors and midplane, facet angles.[24] Using this nomenclature, a facet angle of 90° corresponds to a flat region parallel to the midplane, while a facet angle of 0° indicates a region perpendicular to the midplane.

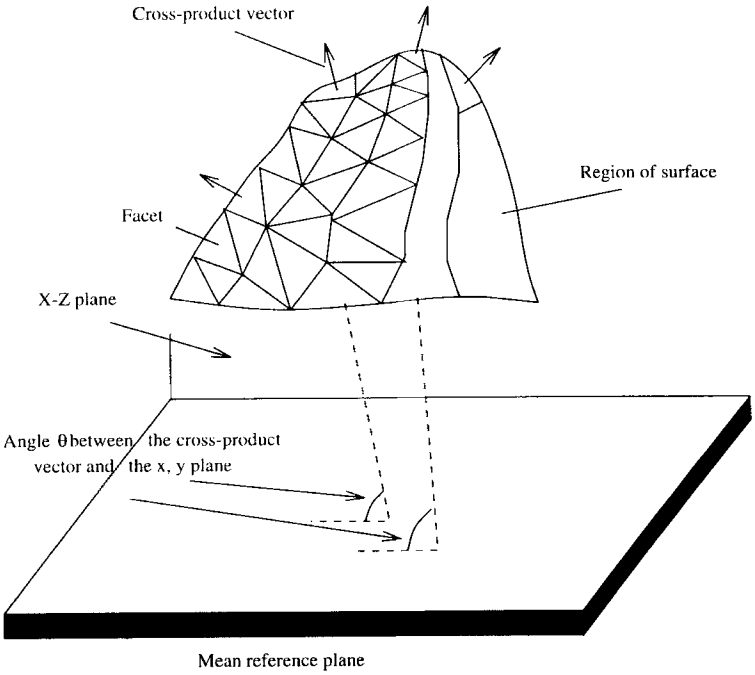

FIGURE 4 Schematic drawing of surface, modelled as a triangular polyhedron. Note the angle θ made by the cross-product vector of two legs of each triangle with the mean reference plane.

(4) Substrate Volumes and Lamina Void Volume Fractions in the Topographic Surface Region

We define the topographic surface region as the region between the planes tangent to the highest asperity, (parallel to the midplane), and that tangent to the lowest point of the area (*i.e.*, $z_{max} - z_{min}$). This should be distinguished from the chemical surface region, where the composition and molecular architecture differs from the bulk (*i.e.*, within the material).

As discussed below, important considerations in relating topographical effects to joint properties may be: (1) variations with depth of substrate volumes from peak asperity heights; and (2) changes in void volume fraction with depth, within the topographic surface region.

Lamina void volume fractions, *i.e.*, the fraction of the volume of each lamina that is devoid of aluminum, were determined as functions of depth. The volume of each lamina was $1\,\mu \times 323.9\,\mu \times 335.8\,\mu = 1.088 \times 10^5\,\mu^3$.

Their determination is straight forward. Each height of the matrix within, or greater than, the designated plane was multiplied by the assigned area $\times$ 1. This equates to the volume of solid material within each lamina. The void volume, V_v, is then the difference between the total volume of the lamina and the volume of solid within the lamina (*i.e.* $V_v = V_T - V_s$). The void volume fraction, $V_{vf} = V_v/V_T = (V_T - V_s)/V_T$.

2. Chemical Characterization

The chemical compositions of the surface regions of samples irradiated with 20 p/reg, CAA-treated and untreated aluminum were determined by Auger electron spectroscopy and Fourier Transform Infra-Red spectroscopy (FTIR). FTIR spectra were obtained in reflectance using a Galaxy Series 2020 Fourier Transform Infra-Red Spectrophotometer (Mattson Instrument Company) having a resolution of $2\,cm^{-1}$. Auger electron spectra were obtained using an ESCA/Auger electron spectrophotometer (Phi Model 548, Physical Electronics Industrial, Inc.). The voltage of the electron gun was 2 KV. The resolution of this instrument is 2 eV.

Spectra were also obtained for the untreated, laser-irradiated, and CAA-treated surfaces after immersion in water for 48 hours and thorough air drying.

III. RESULTS AND DISCUSSION

A. Joint Characteristics

The stress-strain curves for Joint Groups I and II are shown in Figures 3A and B, respectively.

As seen (Fig. 3A), the maximum stresses were about the same for the control and irradiated samples of group I (joints prepared under 175 kPa). The maximum extensions of the irradiated samples were, however, considerably greater. Maximum shear strains for the irradiated joints were roughly double those of the control. The initial (effective) shear moduli for the irradiated joints were, in this case, about 56% ($G = 88.5$ MPa) that of the controls ($G = 157.7$ MPa).

The stress-strain curves for the different subgroups of Group II (joints prepared under 345 kPa) differed from Group I and from each other (Fig. 3B). The ultimate joint (shear) strengths for the irradiated joints were 24% greater than controls and 15% greater than the CAA-treated joints.*

The strains at fracture, for both the irradiated and CAA-treated joints, were around 70% greater than controls. The initial moduli for all three subgroups were, however, about the same. The maximum strains for the treated and control samples of Group II were approximately double those of Group I [Note that the curves do not go through the origin. This is an artifact resulting from the regression analyses used to obtain best fits.]

The stress-strain curves for the irradiated and CAA-treated joints (Group II) were identically linear up to a shear strain of around 0.2. (The linear region for the control joints was limited to around 0.1). At 0.2, the curves for the CAA-treated joints deviated sharply from the laser-treated joints, exhibiting substantially lower stresses on further extension.

* In preliminary studies, joints prepared from coupons treated with 5 p/reg had joint strengths that were 10% less, and strains that were 20% less, than those treated with 20 p/reg. The strain measurements were not, however, determined with an extensometer and are, therefore, not shown in the body of the paper. These measurements were, however, self-consistent.

The deviation of the CAA curves probably resulted from the onset of incipient fracture, (at that strain), with concomitant stress relaxation and plastic deformation occurring on further extension. By contrast, the laser-irradiated joints exhibited greater shear stresses up to about 70% strain level (Fig. 3B), whereupon stress relaxation and plastic deformation likely occurred on further extension.

These data suggest that failure processes began at lower strains with the control and CAA-treated joints than with those subjected to laser radiation. It appears, therefore, that laser radiation can impart greater fracture toughness to joints with the magnitude of the increases dependent on the adhesive used and strain rates attained during deformation.

We believe that there are likely several factors responsible for this. These include; (1) greater interfacial interactions between adhesive and substrate due to the surface oxidation occurring during laser radiation (see below); (2) greater contact area between adhesive and substrate as a result of the topographical changes rendered; (3) lower probabilities for crack initiation; and (4) greater inhibition of crack propagation to failure. The latter two effects, we propose, are a consequence of the topographies formed on radiation (see below). A preliminary, elastic model relating to the latter two effects to topography is presented in Section IV.

The lower moduli, and considerably greater strains at fracture, that were attained with the laser-irradiated joints of Group I in comparison with controls may, however, have been due to other factors. The combined depths of the topographic surface regions for the Group II joints (*i.e.*, $z\,(\max) - z\,(\min)$) were approximately 17% of the adhesive thickness and around 11% for Group I.

Two possible explanations for the Group I deformational properties are as follows. It is conceivable that the surface crevices were not completely filled with adhesive when the joints were prepared at the lower pressure. If such were the case, then the resultant regional contact between adhesive and substrate could result in less restraints at the boundary. This, coupled with less compression of the adhesive matrix, might allow greater stress relaxation during deformation, yielding lower net stresses during straining. This scenario could explain the overall lower moduli observed. Assuming, further, that incipient fracture occurs at some critical stress, then the proposed greater relaxation rates in irradiated joints could have resulted in the attaining of greater strains (compared with the control) prior to fracture. In addition, incomplete filling of the surface crevices could conceivably account for the lower strains at fracture in general for Group I samples compared with Group II samples.

It is, of course, also possible that the surface crevices were filled completely with adhesive even when the joints were prepared at lower pressure. Under these conditions, we would propose, similar to Group II, that the strain gradients within the topographic surface region and between that region and the bulk adhesive are reduced with consequent reductions in the probabilities of crack initiation (see Sect. IV-A). Such a mechanism would explain the greater strains attained prior to fracture for the laser-irradiated surfaces. The lower overall moduli would, however, have to result from effects of the lower strain gradients at the boundaries on the overall strain fields within the adhesive.

There is insufficient evidence, at the moment, to pin down the mechanism. Experiments are planned to determine the extents to which the adhesive fills the surface crevices formed on radiation.

Of further note, based on visual observations, fracture was predominantly cohesive for the laser and CAA joints, whereas the failure mode in the control joints was primarily adhesive. Since the adhesive system used was the same in all cases, it would appear that conditions at the *boundary between adhesive and substrate affected the joints' fracture characteristics even in cohesive failure.*

We should also point out that the 24% increase in joint strength we observed with the irradiated samples of Group II over the controls is less than that observed by Dodiuk *et al.*[17] for their irradiated samples. We attribute this difference to the differences in the adhesives used. The stress-strain curves (Fig. 3A and B) for our irradiated and CAA-treated joints indicate that a considerable amount of plastic deformation occurred during the terminal stages of loading. Once the plastic plateau is reached, further increases in strength would not be expected. It is possible, however, that greater increases in joint strengths can be realized with other adhesives, as a consequence of our laser preparative procedure, and as found by Dodiuk *et al.* for theirs. Note that the maximum fracture stresses attained with this adhesive were considerably greater than those reported by Dodiuk *et al.*.[17]

B. Topographic Characteristics

1. Surface Features of Untreated, Laser Irradiated, and Chromic Acid Anodized Aluminum

Scanning electron micrographs (SEM's) of the surfaces of the untreated aluminum at 300 and 3000X are shown in Figures 5A and 5B. SEM's of the laser irradiated surfaces, for 20p/reg are shown at 30, 100, and 1000X in Figures 6A, B, and C.

Facsimile images (plots of coordinate data) with z axes scaled 9X the x, y axes, are seen in Figures 7, 8 and 9 for untreated aluminum, 5 p/reg and 20 p/reg, respectively.

An SEM of aluminum subjected to Forest Products Laboratory treatment (FPL) and Chromic Acid Anodization (CAA), as delineated in Table I, is seen in Figure 10.

The surface morphology of untreated aluminum is shown to consist of regions of "scaly" indentations, spaced quasi-regularly, across the surface (Fig. 5A). The sharp, scaly features within the regions are more evident at higher magnification (Fig. 5B). Their quasi spatial regularity is also seen in the facsimile image of Figure 7.

Irradiation at 20 p/reg resulted in concentric "circular" wave like structures within each mm^2 region from the center to the periphery (Fig. 6B). At the peripheries there is a "ridge" separating each region (Figs. 6A, 6B, 8 and 9).

At the center of the irradiated areas, there is a quasi-elliptical region, approximately 400 by 500 μ, that has fewer surface oscillations (Figs. 6A, 6B). These are smaller and less distinct with 5 p/reg.

With 20 p/reg the surfaces of the "waves" are relatively smooth. Flow lines are evident but there is no indication of the "porous" structure or high-frequency oscillations seen with CAA-treated surfaces (Fig. 10) nor the "scaly" regions of untreated aluminum (Fig. 5B). Melting and flow apparently "erase" these scaly characteristics.

As stated, around each mm^2 irradiated region there is a rise or barrier between irradiated regions (Figs. 8 and 9). These rises are approximately 8.5 to 12μ above the top of the center of the irradiated regions and approximately 5 μ above the non-

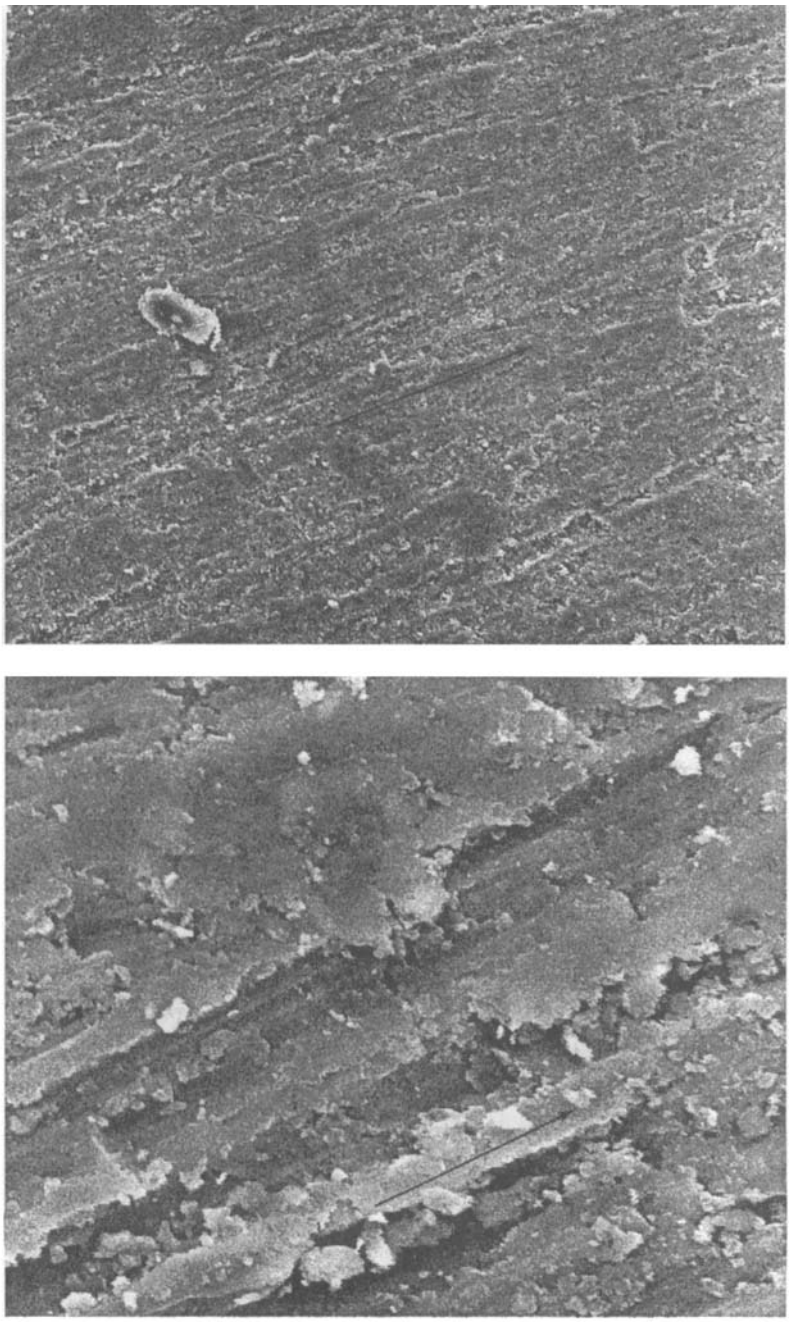

FIGURE 5A and B. SEM of stock aluminum surface at 300 and 3000 X. Note "linear" regions (in direction of arrows) of roughness crossing the surface.

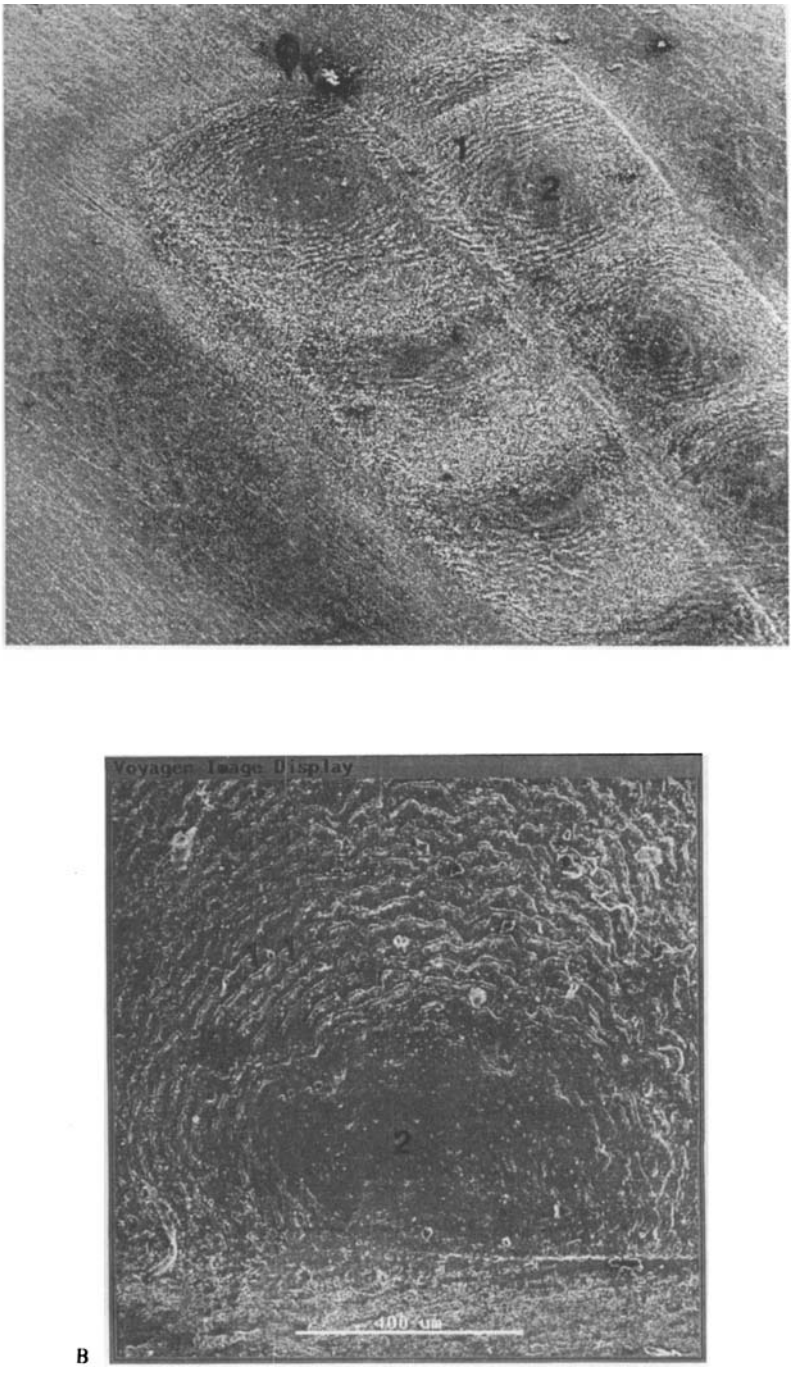

FIGURE 6A, B, C. SEM's of region of aluminum surface after 20 p/reg. Magnifications 30, 100, and 1000 X, respectively. Note patterns within each irradiated area and regularity of wave-like structures (1) distributed elliptically around central region (2). Further note flow lines in Fig. 6C, (3).

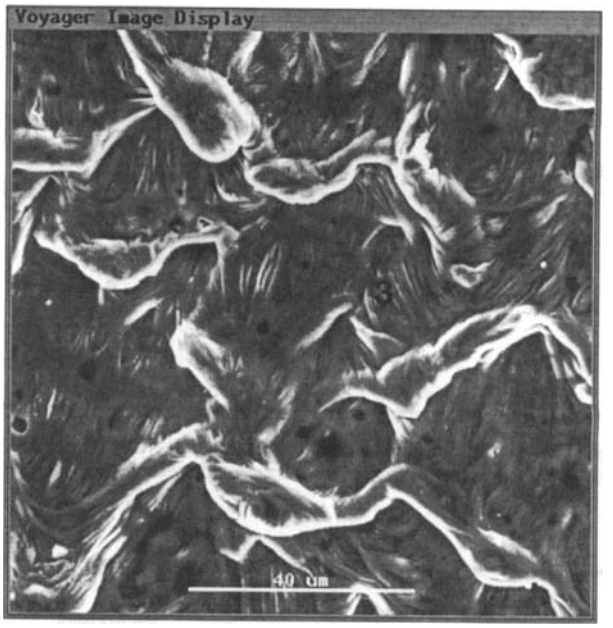

FIGURE 6 *(Continued.)*

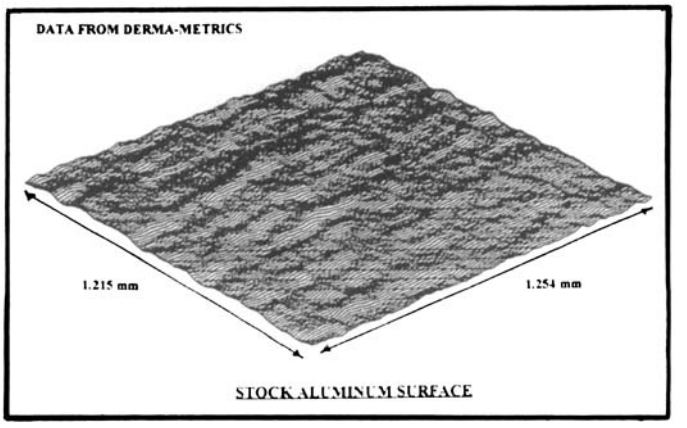

FIGURE 7 Facsimile image of stock aluminum surface. The z axis scaled at 9X the x,y axes to better illustrate features. "Linear" regions of "roughness" across the surface are evident.

irradiated metal when irradiated with 20 p/reg. With 5 p/reg the rises are approximately 3.6 μ above the middle of the irradiated regions and 3 μ above the non-irradiated region. The rises are thought to result from molten flow outward during irradiation. These dimensions, (determined by our mechano-optical system), are the average of 5 to 6 measurements. However, there was a distribution of the heights and thickness of the "walls" across the surface.

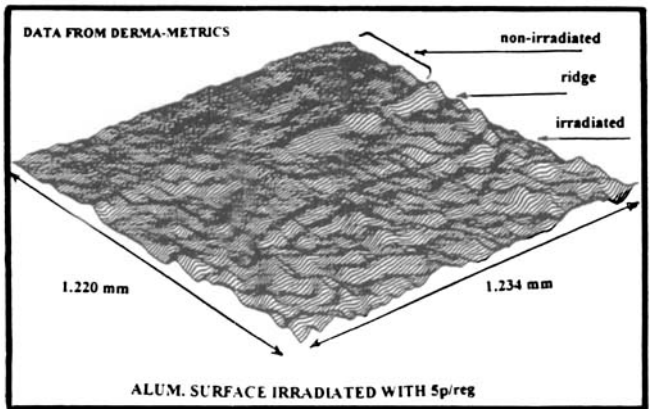

FIGURE 8 Facsimile image of aluminum surface after 5 p/reg. The z axis is scaled at 9X the x, y axes. The beginnings of the "ridge" between irradiated and non-irradiated regions are evident.

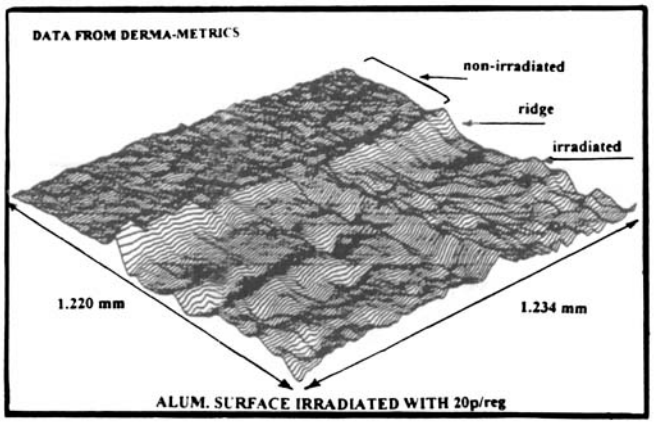

FIGURE 9 Facsimile image of regions of aluminum surface after 20 p/reg. The z axis is scaled at 9X the x, y axes. Note "ridge" separating irradiated regions.

These relatively high walls formed a sort of honeycomb on the surface that possibly could function as crack terminators. Their elimination by an overlapping radiation procedure would permit an assessment of their function.

The incident intensities, as stated, were greater than that required for vaporization. As such, the laser radiation resulted in "losses" of metal due to ablation. The ablated metal was greater for 20 p/reg than 5 p/reg with average depths within irradiated regions being approximately 3.5 to 5 μ below that of the untreated metal. With 5 p/reg they were approximately 2.5 to 3 μ below the untreated metal (see Figs. 8 and 9). These dimensions were likely affected by flow and the redeposition of vaporized metal.

The SEM for CAA-treated stock aluminum (Fig. 10) illustrate "white spots" which are approximately 0.05 μ in diameter and are thought to be the pores on the surface.

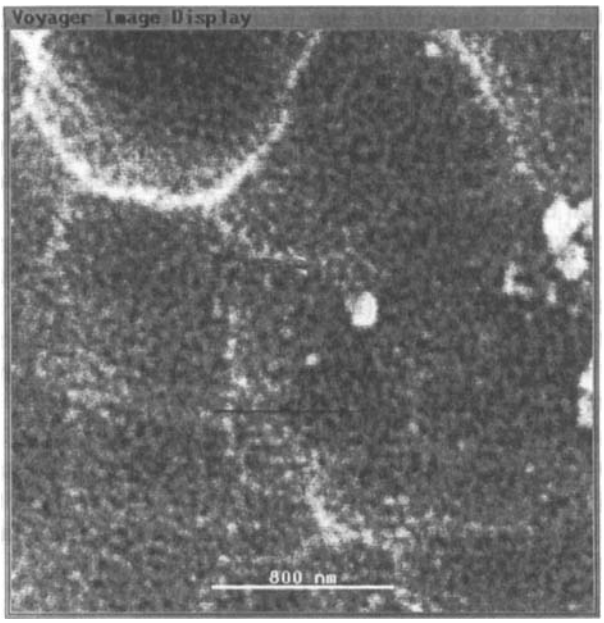

FIGURE 10 SEM (40 K X) of aluminum surface subjected to FPL and CAA treatments. Note the "white spots" (arrow) thought to be the pores on the surface.

These are interpreted as being due to decreased extents of secondary electron emission from the cell bottoms. The CAA surfaces are, therefore, seen to consist of the porous structures described by Venables *et al.*[4] and others.[27] Their diameters are reported[4] to be around 0.04 μ, but these can vary with voltage and electrolyte composition.[28] As such, the spot dimensions seen are of the order of magnitude reported in the literature.

2. *Statistical Characterization of Irradiated Regions*

The topographies of the irradiated aluminum, using these procedures, varied from the center to the periphery of each region. Therefore, the parameters described below represent averaged distributions for the interiors of the irradiated regions. They do not include the region around 10 μ from the peripheral "walls" surrounding each irradiated area.

a. Surface Inclination Distributions

Before discussing these data we should point out that these topographies can be considered to consist of a series of undulations with superimposed frequencies. This would be analogous, on a terrestrial level, to long rolling hills having a variety of undulations within the overall hill structures. Each of these could, in turn, have smaller hillets within their structures, etc. Indeed, Fourier Analysis, although not literally

analogous, is used to characterize the frequency distributions of surface topographies.[28,29]

An understanding of the relationships between topographic characteristics and joint properties, therefore, requires that the relevant frequencies be identified. With 20 p/reg, lower frequency oscillations had somewhat greater amplitudes than those for 5 p/reg. Their inclination distributions were, however, similar at those frequencies but somewhat broader than those for the control.

At frequencies with wavelengths between 1 and 321 μ, (as determined from the Fourier Transforms) the surface inclinations or facet angle distributions for 5 p/reg were broader than those for 20 p/reg (Fig. 11). Surfaces irradiated for 5 p/reg had higher fractions of more-steeply-inclined regions (lower facet angles) than those for 20 p/reg. Thus, while the height distributions for identically spaced data were similar, higher fractions of more-steeply-inclined regions were evident with 5 p/reg.

The greater fractions of higher surface inclinations did not correlate with measurable increases in the stresses or strains at fracture. On the contrary, the stresses and strains at failure for 5p/reg were less than those for 20 p/reg (see footnote for joint characteristics). This is not to say that with other adhesives systems, or other deformation modes, that these inclination differences would not have different effects.

b. Lamina Void Volume Fractions

Variations in void volume fraction with depth are shown in Figure 12 for 5 and 20 p/reg. Changes in void volume fraction with depth are seen to be of sigmoid shape, with average gradients for 20 p/reg being less than those for 5 p/reg. With 20 p/reg, there is a small but significant fraction of deeper, partially-void regions. Note also that at

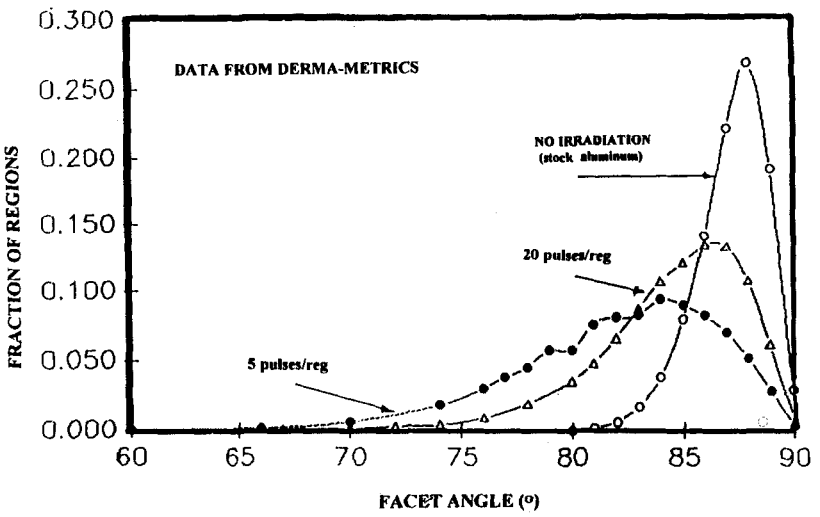

FIGURE 11 Facet angle distributions of stock and laser-irradiated aluminum. Data for interior of irradiated regions spaced 1.27 and 2.54 μ (apart) in x and y directions.

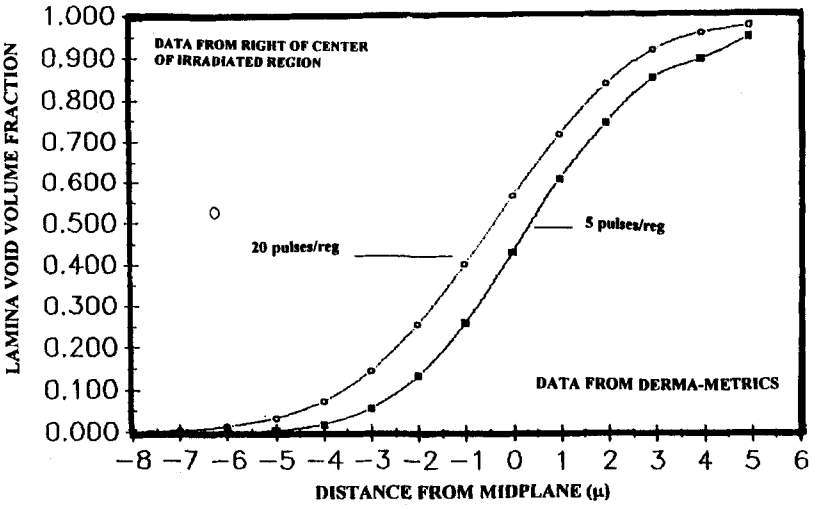

FIGURE 12 Lamina void volume fractions of irradiated aluminum as function of depth.

heights greater than 2.5 μ above the midplane, the void volume fractions are greater than 90%.

These variations in void volume fraction are believed to affect joint fracture. As will be discussed, if the voids are filled with adhesive, we suggest that they: (1) affect the probabilities for crack initiation, through their effect on strain gradients; and (2) the contact area between adhesive and substrate (see Sect. IV).

c. Summary and Discussion of Topographic Characteristics

In summary, the salient characteristics and primary differences between the topographies of irradiated aluminum (20 p/reg) and the other surfaces were: (1) a square grid of "walls" surrounding each irradiated region that were considerably higher than those for 5 p/reg (Figs. 8, 9); (2) greater amplitudes for lower frequency oscillations resulting in greater void volume fractions at lower depths (Fig. 12); (3) a central zone within each irradiated region with fewer undulations ; (Figs. 6A, 6B,and 6C); and (4) higher frequency oscillations having narrower inclination distributions than those for 5 p/reg (Fig. 11).

As to causes, the central zone of each mm^2 region, having fewer undulations, is believed to result from greater extents of ablation and annealing. This may have resulted from the spatial distribution of irradiances incident on the metal.

The wave-like features and overall surface contours of the regions surrounding the central zone probably resulted from a combination of optical effects and flow to the peripheries. The quasi-regular spacing between wave-like structures (Figs. 6A and 6B) suggest mechanisms related to optical effects. Such regularity would not seem likely from flow alone. On the other hand, molten flow is suggested by the greater heights of the peripheral "walls" relative to the unirradiated areas after 20 p/reg as compared with

5 p/reg and the general concavity of the irradiated regions. The SEM of Figure 6C and the facsimile image of Figure 9 exhibit features consistent with flow.

A number of papers in the literature describe different topographical patterns resulting from the laser irradiation of metal surfaces. Some investigators have attributed these effects to mechanisms related to light scattering.[7] Others postulate mechanisms related to interference effects between the incident and reflected light.[7] Still others suggest that topographical changes can be effected by spatial variations in surface tension that are thought to arise from variations in radiation intensity and temperature. These surface tension variations are presumed to cause regional flow with consequent effects on the topography. The transient topographies formed are further thought to be "frozen" when radiation ceases, due to rapid cooling.

We cannot unequivocally state the exact mechanisms by which these surface patterns are generated. More information is required for precise elucidation. We think, however, that the driving force for the observed flow phenomenon could be transient pressure distributions generated over the irradiated area by laser-supported detonation waves (LSDW).[7] These can generate very high surface pressures[7] with resultant shock waves.[7,11] LSDW-related pressure pulses are reported to produce stress waves on target materials resulting in deformation or flow.[7] Calculated pressure contours for systems having irradiances in the range used in this investigation, but at longer time scales, indicate that they decrease quasi-radially from a central region, causing radial flow within the plasma.[7] Assuming that flow of the molten aluminum on the surface relates to flow in the juxtaposed plasma, then a flow field to the peripheries would result. Such flow would explain in part: (1) the general concavity of the irradiated regions; (2) the elliptical distributions of wave-like structures around the central zone; and (3) the walls or rises surrounding each mm^2 irradiated region (Figs. 6A, 6B and 10).

Transient topographies formed from these optical and flow effects are again presumed to be "frozen" be extremely rapid cooling when radiation ceases. Cooling rates of around 10^9°K/s and temperatures within 5 degrees of ambient are calculated[22] to be attained within 0.02 s.

More detailed topographic analyses following irradiation, for pulses between 5 and 20 p/reg, are needed as well as determinations of the aluminum lost during irradiation, to elucidate the mechanisms involved.

The topographies of the aluminum surfaces, reported by Dodiuk *et al.*[17] following irradiation by their procedures, were entirely different from those observed here. Their published SEM's reveal relatively smooth surfaces covered by small holes and fissures around 1 μ long.

These differences are probably due to the considerably lower radiation intensities used by those investigators. Their laser energies ranged between 0.002 and 0.007 J/pulse/mm^2, compared with 0.235 J/pulse/mm^2 in this investigation, (*i.e.*, roughly 0.8 to 3% of ours.). As such, their beam intensities likely ranged between 1.3 and 4.7×10^9 W/m^2, assuming a pulse duration of around 15 ns. This is considerably less than I_m and was, thus, insufficient to ablate or melt the metal.

Interestingly, they reported greater increases in shear strength with laser energies (and consequently laser intensities) that were less than their maximum. Their greatest joint strengths occurred with a laser energy of 0.0018 J/pulse/mm^2, where they state that there were few morphological changes. It would appear, therefore, that their

increased shear strengths resulted primarily from greater interfacial interactions and not from substrate topographical changes. We believe that this was not the case for the procedures used here.

Note that the amplitudes of surface oscillation from our treatments were about two orders of magnitude greater and three orders of magnitude smaller in frequency than those due to CAA. Further, there is no evidence for the porous surface structures described by Venables[4] nor any prevalence of surface fissures with 20 p/mm^2. Nevertheless, the joint characteristics found were at least as good as if not better than, those due to CAA in so far as these tests could detect. We have not, however, evaluated joint durabilities in different environments.

The operative mechanisms by which these topographies affect joint properties are, therefore, thought to be different from those for chemically-prepared surfaces. The topographies of CAA, and other chemically-treated surfaces, are believed to affect joint properties by enhanced interfacial interactions and mechanical entanglement.[4] The higher amplitude topographies attained with our treatment (see Sect. IV) are, by contrast, believed to affect joint properties through enhanced interfacial interaction (Sect. IV) and effects on the strain gradients and crack propagation paths within the adhesive.

C. Surface Chemical Analysis

1. Auger Electron Spectroscopy

The Auger electron spectra in differentiated mode are shown in Figures 13A, B and C for untreated, CAA-treated and laser-irradiated (20 p/reg) aluminum. The characteristic Auger emissions at around 59.5 and 500 eV for aluminum and oxygen are evident.

The ratios of oxygen to aluminum contents can be approximated by the ratio of heights (i.e. h_O/h_{Al}) between peaks in the respective regions of the differentiated curves (*i.e.*, dN/dE *vs* E). These height ratios approximate the ratios of the integrated areas for the respective elements.

The average h_O/h_{Al} values ($\pm$ avg. dev.) for untreated, CAA-treated, and laser-treated aluminum are, respectively, 3.70 ± 0.01, 3.77 ± 0.02, and 4.26 ± 0.08. These data indicate that the relative oxygen contents of the surface regions for both CAA-treated and laser-irradiated aluminum are significantly increased. The higher ratios of oxygen to aluminum for the laser-treated surface are believed to be due, in part, to greater proportions of chemisorbed water, as shown by the FTIR data for the respective surfaces, and the formation of oxyhydroxides.

The overall lower dN/dE values for the laser and CAA-treated surfaces (although not the ratios) may be due to topographical effects. It is possible that their respective topographies result in only fractions of their Auger emissions being detected by the instrument's analyzer. These effects, presumably, cancel in determining the ratios.

The specific oxygen containing moieties of the respective aluminum surfaces are discussed next.

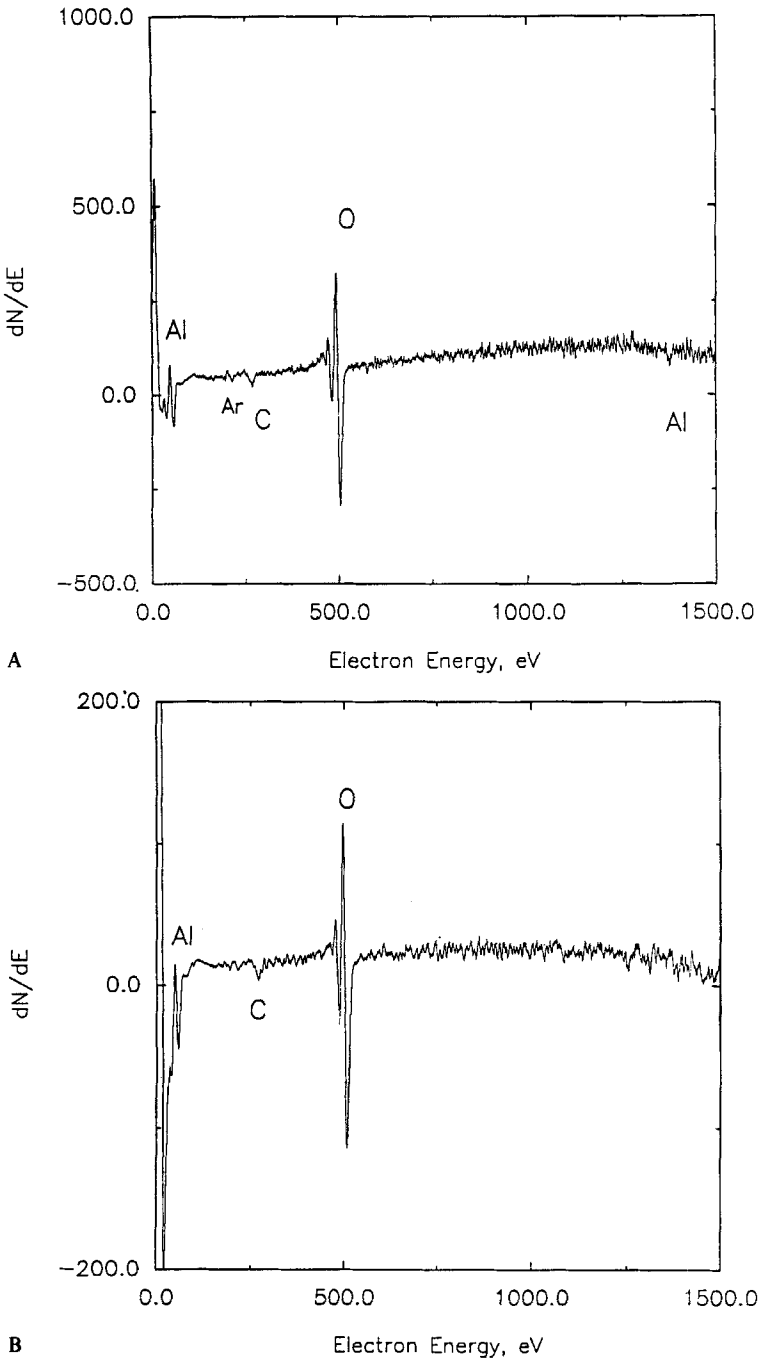

FIGURE 13A, B, C. Auger electron spectra in differentiated mode, for stock aluminum (A) and aluminum irradiated for 5 (B) and 20 p/reg (C).

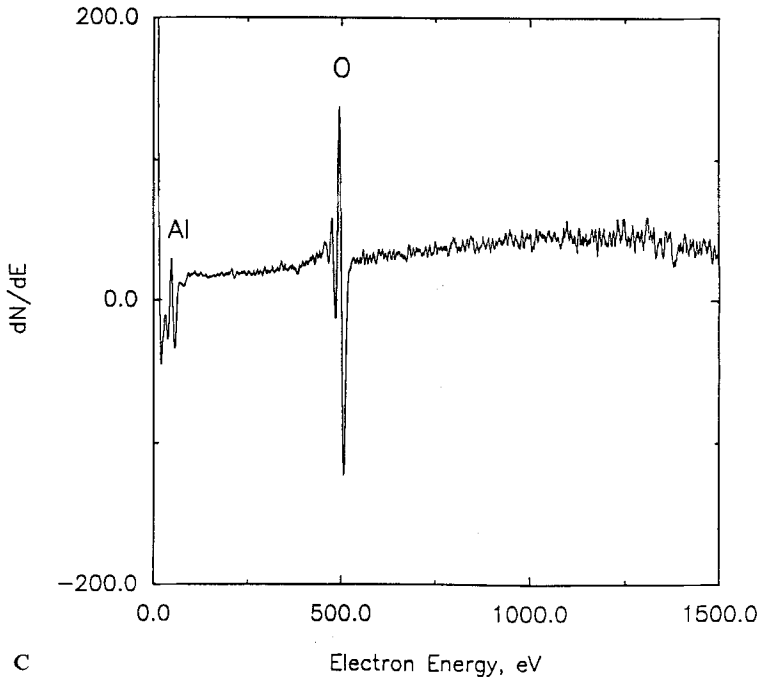

FIGURE 13 *(Continued.)*

2. *Fourier Transform Infra-Red (FTIR) Spectra*

The FTIR spectra for the surface regions of untreated, laser-irradiated (20 p/reg), and CAA-treated aluminum are shown in Figures 14A, B and C respectively. Comparisons of FTIR spectra of these specimens before and after immersion for 48 hours in water are shown in Figures 15A, B and C.

As seen, broad, "continuous" absorption occurs for both CAA-treated and laser-irradiated aluminum in the frequency range from 2500 to 3500 cm^{-1}. By contrast, little absorption is observed in this region for untreated aluminum. Absorptions at these frequencies are attributed to complex distributions of hydroxyl groups that interact through hydrogen bonding.[31]

The functionalities of the hydroxyl groups are, however, different for the CAA-treated as opposed to laser-irradiated surfaces. The surface hydroxyls for the CAA-treated specimen are attributed to a Gibbsite-like structure or $Al(OH)_3$ as evidenced by the very strong absorptions at around 1000 to 1015 cm^{-1}, and the shoulder at around 970 cm^{-1}, which are not present in either the "laser" or "untreated" spectra.[27,31]

The hydroxyl groups of the laser-irradiated surface are, on the other hand, primarily due to a combination of oxyhydroxides (AlOOH) or Boehmite, and chemisorbed water ($Al(OH_2)$). Peaks at 1625 and 1658 cm^{-1}, attributed to adsorbed water, are present in all three spectra, but to much larger extents in the spectra for the laser and untreated surfaces.[31] While the relative absorptivities at these frequencies are somewhat greater for the laser-irradiated surface than for the untreated surface, these differences do not

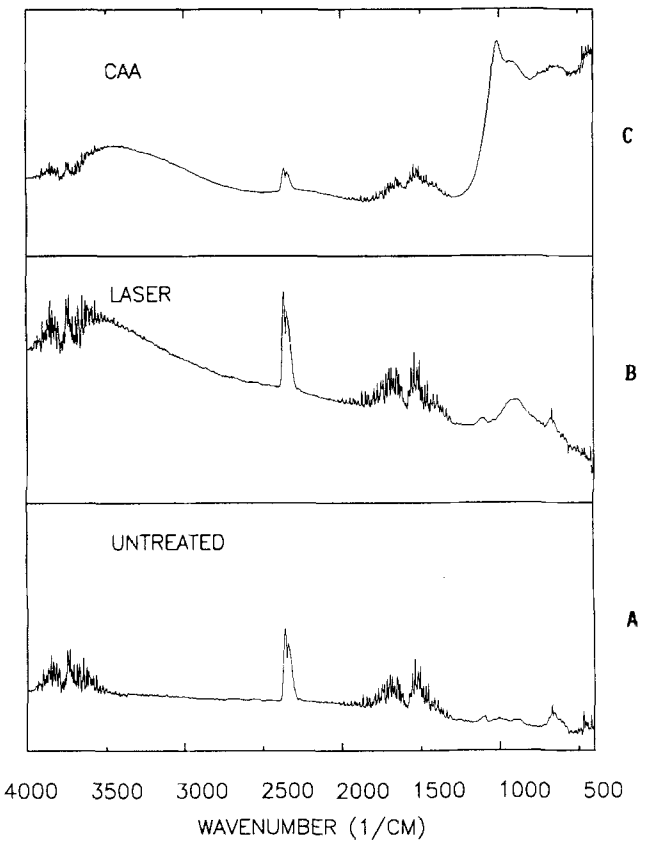

FIGURE 14 Infra-red spectra (in reflectance) for untreated (A), laser-irradiated (20 p/reg) (B), and CAA-treated (C) aluminum.

account for the differences in absorption between 2500 and 3500 cm^{-1}. The presence of oxyhydroxides are further indicated by the absorption at 1080 and 960 cm^{-1}.[27,31]

Boehmite[27,3] is indicated on the laser-irradiated surface by the weak peak at around 1140 cm^{-1}. The moderately strong absorption in the range between 920 and 970 cm^{-1}, seen in the "laser" spectra but not the "untreated" spectra, indicates the presence of Al–O–Al. The peaks at 2338 and 2361 cm^{-1}, present in all spectra, are artifacts due to CO_2.

Immersion in water for 48 hours did not change the spectra for untreated nor CAA-treated aluminum (Figs. 15A and C). The spectrum for the laser-irradiated surface after immersion, however, shows increased absorption in the region between 3200 and 3500 cm^{-1} and at around 1000 cm^{-1}. Decreased absorption at 1080 cm^{-1} (Fig. 15) is also evident. These changes indicate greater concentrations of OH and lower concentrations of oxyhydroxide. They thus likely result from the reaction:

$$AlOOH + H_2O \rightarrow Al(OH)_3 \qquad (2)$$

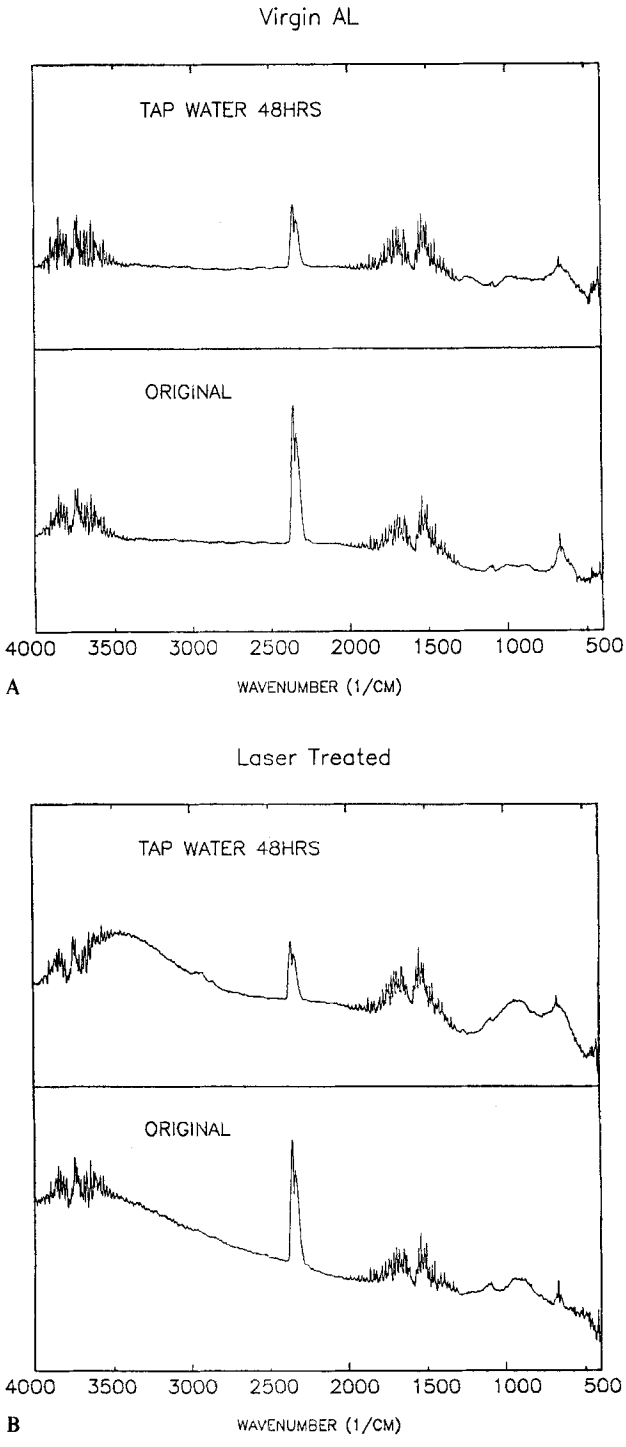

FIGURE 15A, B and C. Comparison of IR spectra of stock aluminum (A), laser-irradiated (20 p/reg) (B), and CAA-treated (C) aluminum before and after immersion in tap water for 48 hours.

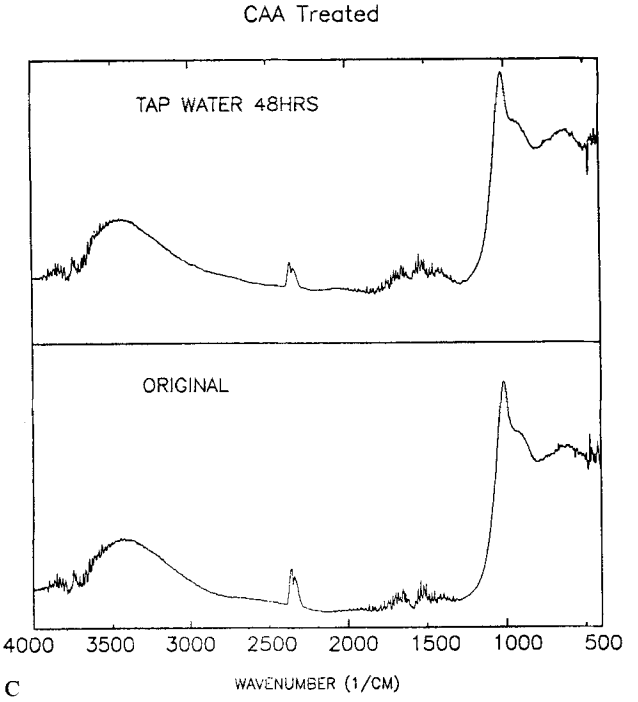

FIGURE 15 *(Continued.)*

The concentrations of surface hydroxides may be increased by irradiation in atmospheres having higher concentrations of oxygen followed by reaction with water.

The IR spectra published by Dodiuk *et al.*[17] for aluminum irradiated at 193 nm, at 0.007 J/pulse/mm^2, are quite different from those found in this investigation for both laser-irradiated and CAA-treated aluminum. The increases in absorption between 2500 and 3500 cm^{-1}, indicative of surface OH, are absent as are the peaks at 1080 cm^{-1} (oxyhydroxides), and the broad peak in the region between 920 and 970 cm^{-1} (Al–O–Al). It is possible that surface hydroxides may have been present at concentrations below that detectable by IR. Clearly the extents of surface oxidation vary with the intensity of irradiance as pointed out by Dodiuk *et al.*[17]

IV. THEORETICAL CONSIDERATIONS

The changes in joint strengths and extensibilities resulting from laser irradiation can be considered from two different (but not mutually exclusive) approaches. These are: (A) a continuum mechanics approach where the constitutive behavior of the resultant bond layer and "interphase" is determined; and (B)a fracture mechanics approach where effects by the "interphase" on the directions of crack propagation and resultant fracture toughness are assessed. These are discussed separately. Although deformation within the bulk adhesive is likely viscoelastic, simple elastic relationships probably suffice to

describe deformation within the topographic surface region. Therefore, simple elastic relationships are used to relate strain gradients within those regions to topography.

A. The Continuum Mechanics Approach

In this approach, the topographic surface region filled with adhesive is modeled as a composite material having moduli that decreases continuously from bottom to top (*i.e.*, from z (min) to the bulk adhesive). The average equivalent elastic modulus, G_{ip}, for the region is determined by assuming that both components of the composite are under an isostress condition. That is, both metal and adhesive are under the same shear stress, τ_{ip}. The composite interfacial shear strain, γ_{ip}, is assumed equal to the volumetric weighted average of the adhesive and adherend strains, *i.e.*:

$$\gamma_{ip} = V_{fA}\gamma_A + V_{fs}\gamma_S \tag{3}$$

In equation (3) γ_A and γ_S are the adhesive and substrate shear strains and V_{fA} and V_{fS} are the volume fractions of adhesive and substrate for the region. Assuming that the adhesive essentially fills the voids, the adhesive volume fraction can be equated to the sum of the void volume fractions of each lamina shown in Figure 12. The substrate volume fraction, V_{fS}, is equal to $1 - V_{fA}$.

If deformation of both adhesive and adherend are, as a first approximation, assumed to be elastic, we can define the interphase shear modulus as

$$G_{ip} = \tau_{ip}/\gamma_{ip} \tag{4}$$

Using equations (3) and (4) and Hooke's law to represent the behavior of the adhesive and adherend, we obtain an expression for the interphase shear modulus:

$$G_{ip} = G_S G_A (V_{fA} G_S + V_{fS} G_A)^{-1} = G_S G_A [V_{fA}(G_s - G_A) + G_A]^{-1} \tag{5}$$

where G_A and G_S are the elastic moduli for adhesive and adherend, respectively.

We now make the reasonable assumption that failure in the interphase is more likely with higher shear strain gradients. In the limit, strain discontinuity defines failure, based on mechanics principles. Using this premise, we derive a mathematical expression that assesses relative failure probability in the region, by relating the shear strain gradients to the shear moduli of the adhesive and adherend, and the volume fractions of adhesive. For this purpose, we differentiate equation (4) with respect to z, *i.e.*, the thickness of the topographic surface region:

$$\frac{dG_{ip}}{dz} = -\tau_{ip}\gamma_{ip}^{-2}\left(\frac{d\gamma_{ip}}{dz}\right) \tag{6}$$

An equivalent expression is obtained by differentiating equation (5) with respect to z:

$$\frac{dG_{ip}}{dz} = -G_S G_A (G_S - G_A)[V_{fA}(G_S - G_A) + G_A]^{-2}\frac{dV_{fA}}{dz} \tag{7}$$

Equating equations (6) and (7) we obtain an expression relating the shear strain gradient, $d\gamma_{ip}/dz$, to the average volume fraction of adhesive, V_{fA}, and the differential void volume fraction dV_{fA}/dz. Both parameters were, as shown, experimentally determinable (Fig. 12).

Thus, surface morphology effects on joint properties are proposed not only to increase interfacial interactions but also to: (1) affect strain gradients at the interphase; and (2) crack propagation paths within the adhesive (as discussed in the next section). While the model is, as stated, a first approximation that undoubtedly requires modifications as more information is obtained, it is clear that the proposed mechanisms require specific macrotopographical characteristics of the adherend, in addition to chemical interactions, to effect increased fracture toughness. As such, the proposed mechanisms differ from those presumed to be operative with the microtopographical changes rendered by CAA (and other etching procedures), or with the topographies generated by the relatively low energy radiation procedures used by Dodiuk *et al.*[17].

B. Fracture Mechanics Considerations

The second mechanism by which these topographies are proposed to affect fracture toughness are through their effects on crack propagation paths and crack terminations under the ensuring mixed-mode conditions (Fig. 16). This discussion is based on the maximum principal stress criterion predicting the directions of crack propagation.

For monotonic mixed-mode fracture of structural (epoxy) adhesives in the bonded form, Sancaktar *et al.*[32,33,24] determined that the maximum principal stress criterion provides a better correlation in predicting failure. This criterion predicts failure in mode I (cleavage) under the action of the maximum principal stress since a biaxial state

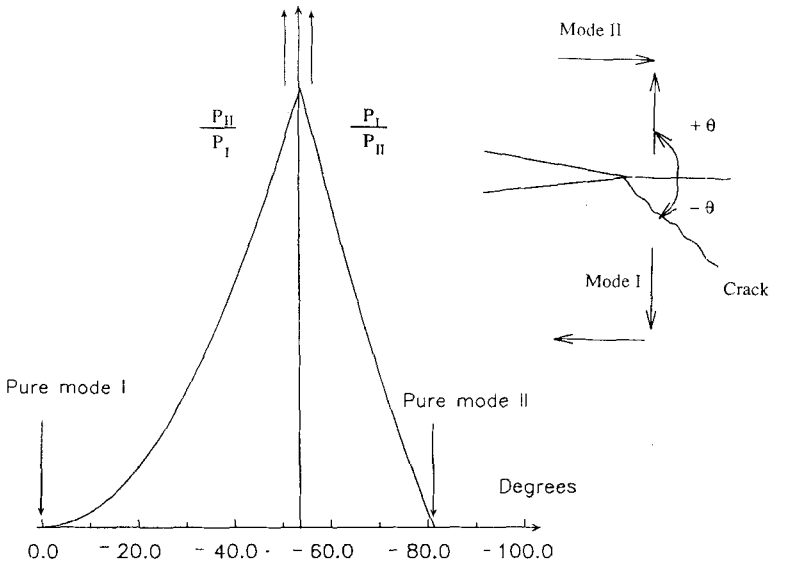

FIGURE 16 Schematic diagram of Modes I and II and ratios as functions of stress direction.

of stress is applied globally. The mode I in such cases will be at an angle to the applied P_I load, with this angle being determined by the applied P_I to P_{II} ratio (Fig. 16). Obviously such an inclined crack will have to connect with similar ones or simply continue propagating in the P (shear) direction, close to or at the interface, to result in catastrophic failure. The likelihood of this type of failure is especially high for brittle adhesives. Consequently, the different facet angles created on the substrate surface by these laser radiation procedures are expected to affect this mixed-mode behavior since cracks are not able to propagate into the metal adherend.

The availability of facet angle distributions, at various frequencies, as shown in Figure 11, therefore provide means of modeling crack propagation directions that could presumably result in changes in apparent toughness. It remains for future work to relate these model predictions of fracture toughness to fracture surface topographies.

V. CONCLUSIONS

1. The stepwise radiation of mm^2 regions of aluminum adherends with a KrF eximer laser (248 nm) in air, at an average intensity of 1.67×10^{13} W/m^2/pulse, (for 20 p/reg), was shown to result in a 24% increase in the ultimate strength values for symmetrical lap joints (using a commerical epoxy adhesive) in comparison with non-treated surfaces. The ultimate strength values were 15% greater than those for chromic acid anodized (CAA) surfaces, using this adhesive system. The strains at fracture for the laser-irradiated surfaces were 69% to 97% greater than those for the non-treated surfaces, depending on the cure pressure. The larger difference corresponded to lower cure pressure (175 kPa). While the methodology is not optimized, the use of such laser radiation for the surface preparation of adherends shows great promise in replacing the chemical methodologies presently used, since the latter are environmentally hazardous.

2. The laser radiation results in significant surface oxidation (as determined by FTIR) with the formation of oxyhydroxides and alumina. The oxyhydroxides can be converted to surface hydroxides by immersion in water. The laser radiation thus simultaneously changes the surface chemistry and topographies of the metal.

3. The topography of each irradiated area consists of a central elliptical region, approximately $400 \times 500\,\mu$, that is essentially devoid of surface osciallations. This is surrounded by a region having quasi-regularly spaced "waves" that "advance" towards the peripheries in all directions. At the peripheries are walls or rises separating the irradiated regions, extending approximately $5\,\mu$ above the non-irradiated metal, when 20 p/reg is used.

The topographies of the surfaces were qualitatively characterized by SEM and quantitatively by a mechano-optical system described herein. Using the mechano-optical system, the volumes of aluminum above designated planes within the topographic surface region were determined, together with the void volume fractions of laminas within that region. [The topographic surface region is defined as $(z\,(\max) - z\,(\min))$]. In addition, height and inclination distributions were determined. Parameters derived from experimentally-determined lamina void volume fraction distributions and volume fractions of adhesive within the topographic surface region

were put into a theoretical framework. These are proposed to govern the mechanisms by which these surfaces enhance the fracture toughness of joints.

4. These surface characteristics are proposed to increase fracture toughness by: (1) increasing interfacial interactions between adhesive and metal through chemical oxidation; (2) minimizing the probabilities of crack initiation through the minimization of strain gradients within the topographic surface region and between that region and the bulk adhesive; and (3) by altering crack propagation paths within the adhesive such that initiated cracks terminate prior to catastrophic failure. As such, it is proposed that the operative mechanisms for attaining fracture toughness differ from those for CAA-treated surface, as revealed by the corresponding stress-strain diagrams.

Acknowledgements

Financial support by New York State Science and Technology Foundation through Clarkson University's Center for Advanced Materials Processing (CAMP) is gratefully acknowledged.

The authors would also like to thank Dr. Richard Stillwell of Derma-Metrics for valuable discussions and Mr. W. Ma for obtaining some of the initial SEM and joint data.

References

1. H. M. Clearfield, D. K. McNamara and G. D. Davis, *Engineered Materials Handbook*, Vol. 3, H. F. Brinson, Ed. (ASM International, Materials Park, OH, 1990), p. 259.
2. R. F. Wegman, *Surface Preparation Tehniques for Adhesive Bonding* (Noyes Publishers, Park Ridge, NJ, 1989).
3. E. W. Thrall and R. W. Shannon, *Adhesive Bonding of Aluminum Alloys* (Marcel Dekker Inc., New York, NY, 1985).
4. J. D. Venables, *J. Mater. Sci.*, **19**, 2431 (1984).
5. W. W. Duley, *Laser Processing and Analysis of Materials* (Plenum Press, New York, 1983).
6. E. A. Metzbower, *Applications of Lasers in Materials Processing* (ASM International, Materials Park, OH, 1979).
7. M. V. Allman, *Laser Beam Interactions with Materials*, Springer Series in Materials Science 2, (Springer Verlag, New York, NY, 1986).
8. M. V. Allman, *Laser and Electron Beam Processing of Materials*, C. W. White and P. S. Peercy, Eds. (Academic Press, New York, NY, 1980).
9. V. E. Fortov, V. V. Kostin and S. J. Eliezer, *J. Appl. Phys.*, **70**(8), 4524 (1991).
10. H. Badekas, A. Koutsomichalis and C. Pangoupoulis, *Surface and Coatings Technology*, **34**, 365 (1988).
11. B. Jackenath, H. Durchalz, H. W. Bergmann and J. Dembowski, *Eximer Lasers and Applications*, Proceedings of SPIE, 1988, Vol. 1023, p. 236.
12. G. Kinsman and W. W. Duley, *Laser Beam Surface Treating and Coating*, Proceedings of SPIE, 1988, Vol. 957, p. 105.
13. R. F. Wood, J. C. Wang, G. F. Gilee and J. R. Kirkpatrick, *Laser and Electron Beam Processing of Materials*, C. W. White and P. S. Peercy, Eds. (Academic Press, New York, NY, 1980), p. 37.
14. S. T. Picraux and L. E. Pope, *Science*, **226**, 615 (1984).
15. R. Kelly and J. C. Rothenberg, *Nuclear Instruments and Methods in Physics Research*, **B7**, 755 (1985).
16. I. Ursu, I. N. Mihailescu, L. C. Listor, V. S. Teodorescu, A. M. Prokhorov, V. I. Konov and S. A. Uglov, *J. Phys. D.*, **20**, 1519 (1987).
17. H, Dodiuk, A. Buchman, S. Kenig, M. Rotel, J. Zahav and T. J. Reinhart, *J. Adhesion*, **41**, 93 (1993).
18. A. Kasuya and Y. Nishina, in *Laser Ablation for Material Synthesis*, Materials Res. Soc. Symp. Proc., Vol. 191, D. Paine and J. C. Bravman, Eds. (Mat. Res. Soc., Pitts., PA, 1990), p. 73.
19. L. Wiedeman and H. Helvayian, *ibid.*, p. 217.
20. D. H. Auston, L. M. Scorko, J. C. Venkatesan, R. E. Slusher and J. A. Golovchenko, *Appl. Phys. Letters*, **33**, 437 (1978).
21. J. S. Horwitz, D. B. Chrisey, M. S. Osofsky, K. S. Grabowski and T. A. Vanderah, in *Laser Ablation for Material Synthesis*, Material Res. Soc. Symp. Proc., Vol. 191, D. Paine and J. C. Bravman, Eds. (Mat. Res. Soc., Pitts., PA, 1990), p. 223

22. T. R. Jervis, T. G. Zocco, K. M. Hubbard and M. Nastasi, *Metallurgical Transactions*, **24A**, 215 (1993).
23. E. M. Breinon and B. H. Keal, *Laser Material Processing*, M. Bass, Ed. (Elsevier North Holland Publishing Co., New York, NY, 1983) p. 242.
24. H. Lipshitz, M. Bridger and G. Derman, *TAPPI J.*, **73**, 237 (1990).
25. H. Lipshitz, U. S. Patent, No. 5, 125, 746 (June 30, 1992).
26. E. Sancaktar and H. F. Brison, in *Adhesion and Adsorption of Polymers*, Vol. 12A, L. H. Lee, Ed. (Plenum Press, NY, 1980), p. 279.
27. K. Wefers, *et al.*, *Oxides and Hydroxides of Aluminum*, Alcoa Technical Paper, No. 19, (Alcoa Laboratories, Pittsburgh, PA, 1987), p. 69.
28. P. P. Nayak, *Trans. ASME, J. Lub. Tech.*, **93F**, 398 (1971).
29. T. R. Thomas, *Rough Surfaces* (Longman, London, 1982), p. 109.
30. C. Herzuger and E. W. Kreutz in *Laser Processing and Diagnostics*, D. Bauerk, Ed. (Springer-Verlag, New York, Ny 1984), p. 90.
31. F. Fondeur and J. L. Koenig, *J. Adhesion*, **40**, 189 (1993).
32. E. Sancaktar, H. Jozavi, J. Baldwin and J. Tang, *J. Adhesion*, **23**, 223 (1987).
33. E. Sancaktar, in *Engineered Materials Handbook*, Vol. 3, H. F. Brinson, Ed. (ASM International, Materials Park OH, 1990), p. 501.
34. E. Sancaktar and J. Tang, *Proc. Adhesion, 87*, (Plastic and Rubber Inst., London, 1987), p. 18-1